ACS APPLIED MATERIALS & INTERFACES

Research Article

www.acsami.org

High-Resolution, High-Aspect Ratio Conductive Wires Embedded in Plastic Substrates

Ankit Mahajan,[†,§] Woo Jin Hyun,[†,§] S. Brett Walker,[‡] Jennifer A. Lewis,[‡] Lorraine F. Francis,*[,†] and C. Daniel Frisbie*[,†]

[†]Department of Chemical Engineering and Materials Science, University of Minnesota, 421 Washington Avenue S.E., Minneapolis, Minnesota 55455, United States

[‡]School of Engineering and Applied Sciences, Wyss Institute for Biologically Inspired Engineering, Harvard University, Cambridge, Massachusetts 02318, United States

Supporting Information

ABSTRACT: A novel method is presented to fabricate high-resolution, high-aspect ratio metal wires embedded in a plastic substrate for flexible electronics applications. In a sequential process, high-resolution channels connected to low-resolution reservoirs are first created in a thermosetting polymer by imprint lithography. A reactive Ag ink is then inkjet-printed into the reservoirs and wicked into the channels by capillary forces. These features serve as a seed layer for copper deposition inside the channels via electroless plating. Highly conductive wires (>50% bulk metal) with minimum line width and spacing of 2 and 4 μm, respectively, and an aspect ratio of 0.6 are obtained. The embedded wires exhibit good mechanical flexibility, with minimal degradation in electrical performance after thousands of bending cycles.

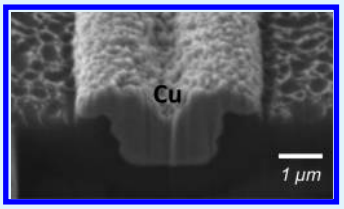

KEYWORDS: *high-resolution metal lines, imprint lithography, inkjet printing, copper electroless plating, flexible electronics*

1. INTRODUCTION

Integration of electronics in flexible, large-area formats is central for emerging applications, such as biosensing, drug-delivery, information displays, identification tagging, and inventory tracking.[1−4] Conductive wires are essential elements of electronic circuitry, and high-resolution, high-conductivity traces are crucial for achieving high-density, faster devices.[1] Large-area formats require longer wires, which lead to higher resistances. Because high-density circuitry constrains wire widths, the ability to pattern high-aspect ratio (height/width) traces is essential. The ability to embed wires within plastic substrates would yield planarized circuitry ideally suited for subsequent processing steps (e.g., coating a thin organic film on top of the wires).[5−8]

High-throughput printing methods, such as flexography, gravure, offset, and screen printing, are widely used for patterning large-area electronic devices.[9] However, a general drawback of these techniques is poor resolution, low-aspect ratio (<0.1), and inhomogeneities in layer thickness. Recently, high-resolution (<10 μm) gravure-printed Ag lines have been demonstrated,[10,11] but line consistency remains a concern, particularly for these fine features. Inkjet printing of metal lines from a diverse array of inks, including nanoparticle, metal−organic decomposition, or particle-free solutions, has also been demonstrated.[12−15] However, the minimum width of inkjet and aerosol-jet printed features is ∼20 μm,[16] due to limits on droplet diameter and spreading on the substrate upon impact. Although Sekitani et al.[17] have demonstrated 2 μm Ag lines using sub-femtoliter inkjet-printed droplets, multiple passes were required to obtain the desired metal content in the wires.

Here, we present a robust, low-temperature, and liquid-based patterning method for obtaining high-resolution and high-aspect ratio metal lines embedded in a plastic substrate that combines three steps: (1) imprint lithography (I),[18] (2) inkjet printing (P),[19] and (3) electroless plating (P).[20] We refer to this method by the acronym, IPP. In IPP, first, microchannels connected to reservoirs are molded into a coated thermoset material using imprint lithography. Next, using a drop-on-demand inkjet printer, a reactive Ag ink is delivered into the reservoir, which flows into the microchannel via capillarity resulting in a thin Ag trace upon annealing. Subsequently, the channel is filled completely with metal by immersing the substrate in a Cu electroless plating bath, where the Ag inside the microchannels serves as a catalyst for selective deposition of Cu.

2. RESULTS AND DISCUSSION

Figure 1 shows a series of steps involved in the IPP process. First, a master template is fabricated by etching reservoirs and channels in a silicon substrate (Supporting Information, Figure S1a). The width of the channels ranged from 1.5 to 100 μm, whereas the reservoirs are 400 μm in diameter. The master template, in turn, is used to create a polydimethylsiloxane (PDMS) "daughter" stamp (Supporting Information, Figure S1b). The stamp is then pressed into a curable epoxy prepolymer liquid coated on a polyethylene terephthalate

Received: October 30, 2014
Accepted: January 5, 2015
Published: January 16, 2015

DOI: 10.1021/am507539a
ACS Appl. Mater. Interfaces 2015, 7, 1841−1847

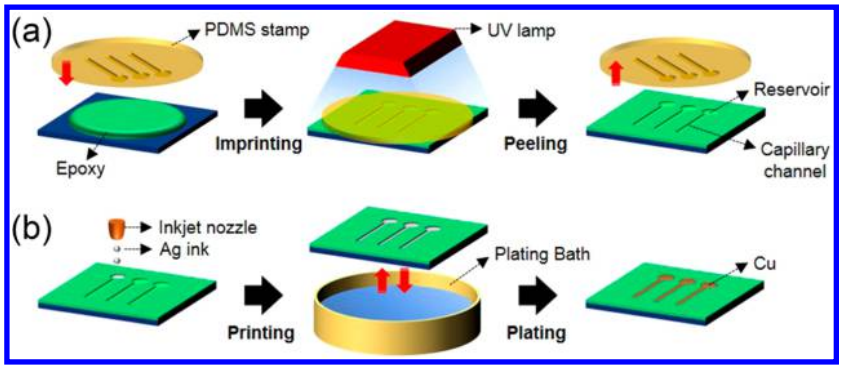

Figure 1. Scheme showing IPP process steps. (a) Fabrication of a flexible, imprinted substrate by pressing a PDMS stamp into a PET substrate coated with a curable epoxy prepolymer, solidifying the coating by UV illumination, and peeling the stamp after the coating is completely cured. (b) Creation of high-resolution and high-aspect ratio metal wires by first inkjet printing of a reactive Ag ink into the microimprinted reservoirs. Capillary flow drives the ink into and along the microchannels. Finally, the channels are completely filled with metal by immersing the printed substrate in a Cu electroless plating bath.

(PET) film pretreated by plasma to enhance the adhesion between the epoxy coating and the substrate. The prepolymer is cured using UV illumination, following which the stamp is delaminated to yield imprinted reservoirs and channels on the epoxy-coated PET substrate.

Next, a reactive silver ink[15] is deposited into the reservoirs using a drop-on-demand inkjet printer, where it is wicked along the channels via capillary forces. Unlike flat substrates, spreading of this low-viscosity ink is confined only to the width of the channel. Upon drying and annealing of this ink, a thin deposit of Ag is left behind in the reservoir and the channel.[21] These channels are filled completely by immersing the substrate in a Cu electroless plating bath, where the Ag inside the microchannels serves as a seed layer for selective deposition of Cu. In the final configuration, the filled microchannels serve as conductive wires, whereas the reservoirs serve as contact pads (Supporting Information, Figure S2).

A particle-free, reactive Ag ink is used to create the seed layer, whose rheological properties are tailored to simultaneously facilitate inkjet printing and capillary flow (see Supporting Information for details). This ink is devoid of any organic binder. The surface of Ag metal obtained postannealing is free from any organic residue, hence serving as an excellent seed layer for Cu growth, as discussed later. Figure 2a shows a plan-view scanning electron micrograph (SEM) of a 50 μm wide channel filled with Ag metal. The Ag ink remains confined within the channel during the wicking process. The controlled nature of capillary flow ensures that the lands are residue-free, which is an advantage over other trench-filling methods (e.g., doctor blade filling[22,23]). The two leading edges near the termination of flow are also distinguishable, suggesting that for the entire duration of capillary flow, the bulk liquid trailed the liquid along the sidewalls. As the Ag ink in the reservoir approached the capillary channel, the liquid was first imbibed along the two corners of the channel forming a curved meniscus, leading to a pressure gradient between the reservoir and the channel (i.e., the capillary pressure, ΔP).[24] Capillary pressure in the direction of flow in an open, rectangular channel can be described as[25]

$$\Delta P = \gamma(\cos\theta)\left(\frac{1}{d} + \frac{2}{w}\right) \quad (1)$$

where γ is the surface tension of the liquid, θ is the contact angle of the liquid on the walls of the channel, and d and w are

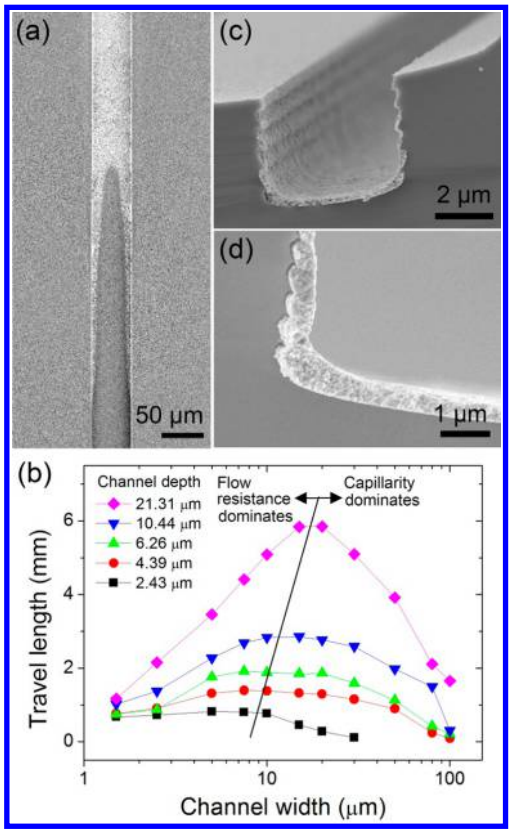

Figure 2. Capillary filling of Ag ink in microchannels. (a) Top-view scanning electron micrograph showing the termination point of the Ag ink inside a 50 μm wide, 10 μm deep imprinted channel on a plastic substrate. (b) Variation of Ag ink travel length with different channel depths and widths. The total length of the channels was 5 cm. Cross-sectional SEM displaying (c) Ag metal deposited on the sidewalls and bottom of a 5 μm wide channel post drying and annealing of the ink, and (d) region of increased Ag thickness near one of the bottom corners of a channel.

depth and width of the channel, respectively. This pressure gradient drives ink flow down the channel against the competing flow resistance arising from friction at the channel walls.[26]

To investigate the effect of channel geometry on the travel length, the reactive Ag ink, with a volume equivalent to reservoir volume, was introduced and flowed within long (5

DOI: 10.1021/am507539a
ACS Appl. Mater. Interfaces 2015, 7, 1841−1847

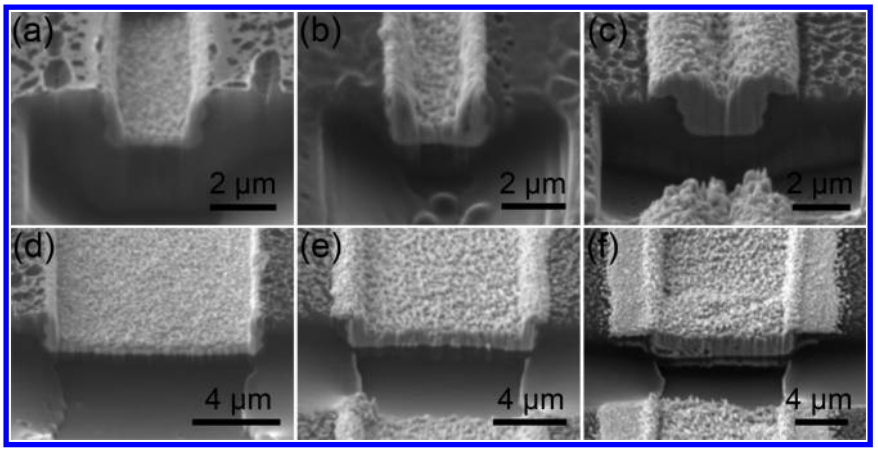

Figure 3. Electroless plating of Cu in printed microchannels. Focused ion beam cross sections showing Cu growth in a 2.5 μm wide channel after (a) 3 min, (b) 6 min, and (c) 9 min of immersion in the plating bath, and a 10 μm wide channel after (d) 3 min, (e) 6 min, and (f) 9 min of immersion. The depth of the channel in both the cases is 2.5 μm.

cm) channels of varying widths and depths (Figure 2b and Supporting Information, Figure S3). Beginning with the widest channels, as shown on the right in Figure 2b, travel length initially increased upon decreasing the channel width at a constant channel depth. However, for narrow channels (<15 μm), the opposite trend occurred, as discussed below. Travel length also increased upon increasing the channel depth at any constant value of width. For a continual supply of liquid to a closed capillary channel, liquid flow never terminates, although the speed of the advancing liquid front continuously decreases along the channel length.[27] By contrast, in open channels, the movement of the ink is also accompanied by solvent evaporation, which results in a localized increase in viscosity at the advancing liquid front (the part that exists in the channel for the longest duration). Eventually, this liquid front completely solidifies, and further ink flow is inhibited. Once formed, the solidification front advances inward toward the reservoir.

The travel length of the reactive silver ink in an open channel can be roughly estimated as the product of the average flow velocity and the time at which solidification sets in at the advancing liquid front. The onset of solidification depends upon the vapor pressure of the ink and height of the liquid inside the channel but not on channel width (exposed surface area to volume ratio of liquid in channels with different widths but same depth is constant). The average flow velocity, on the other hand, has a strong dependence on the width of the channel. Decreasing the channel width, while maintaining a constant depth, enhances capillary pressure (from (eq 1)). However, flow resistance also increases upon decreasing the width, with the effect being especially pronounced in very narrow channels. Resistance to flow in a closed microchannel of width w is inversely proportional to w^4;[26,28] hence, a similar dependence can also be expected for open microchannels. Therefore, average flow velocity increases and subsequently decreases upon decreasing the channel width for a fixed depth, dictated by the relative dominance of either capillary pressure or flow resistance, respectively (Figure 2b). Interestingly, the travel length increases upon increasing the channel depth, for a constant width. Although increasing the channel depth decreases capillary pressure (from (eq 1)), it also reduces the effect of viscous dissipation from the channel floor, besides increasing the time for solidification at the advancing liquid front. Therefore, both flow velocity and travel time of the ink increase in deeper channels. It is worthwhile noting that maximum travel length observed for our experiments is close to 6 mm, which should be adequate for most printed circuits applications. Work is underway to increase this travel length by further reducing the initial ink viscosity and suppressing evaporation during the ink migration process.

Cross-sectional SEM provides insight into the dynamics of flow and drying of the Ag ink inside a microchannel. Figure 2c reveals that a thin Ag deposit is present on both the sidewalls and bottom of a 5 μm wide channel. The presence of Ag on the sidewalls indicates that during the entire capillary flow, the liquid filled the channel almost to the top.[29] It is also testimony to the pinning of the contact line to the top of the walls during drying. Similar to the coffee-ring effect on flat surfaces,[30] the pinned contact line initiates liquid flow from the center toward the wall during drying, leading to a region of slightly increased Ag thickness near the walls and a region of uniform thickness away from the walls (Figure 2d). This is consistent with results obtained for polymer and latex solutions dried within similar confined geometries.[31,32]

Capillary filling enables patterning of the reactive Ag ink in high-resolution channels. However, the channels are only partially filled with metal after drying and annealing of the ink. To obtain high-aspect ratio conductors, complete filling of the channels with metal is required. This is accomplished by electroless deposition of Cu. Upon immersing the substrate in the plating solution, Cu ions from the solution diffuse toward the Ag metal inside the microchannels, where they are reduced to Cu metal.[20] Figure 3 displays focused ion beam (FIB) cross sections, which illustrate time-dependent growth of Cu inside Ag-filled microchannels (widths: 2.5 and 10 μm, depth: 2.5 μm). The temperature of the bath is maintained at 55 °C. After 3 min of immersion, Cu grows exclusively atop Ag present on both the sidewalls and the bottom of the channel (Figure 3a,d). The thickness of Cu increases with plating time, with an average growth rate of ~300 nm min^{-1}. Interestingly, side overgrowth near the top of the channel sidewalls is also seen after a plating time of 6 min, indicating isotropic growth of Cu around an individual Ag seed (Figure 3e). Eventually, after 9 min, both the 2.5 and 10 μm channels are flush with Cu with an overgrowth of 0.8 and 3 μm, respectively, on either side of the channel (Figure 3c,f). Advancing Cu metal fronts from both the sidewalls and the bottom seamlessly merged to completely fill the channels, yielding very high-aspect ratios (height/width) of

DOI: 10.1021/am507539a
ACS Appl. Mater. Interfaces 2015, 7, 1841−1847

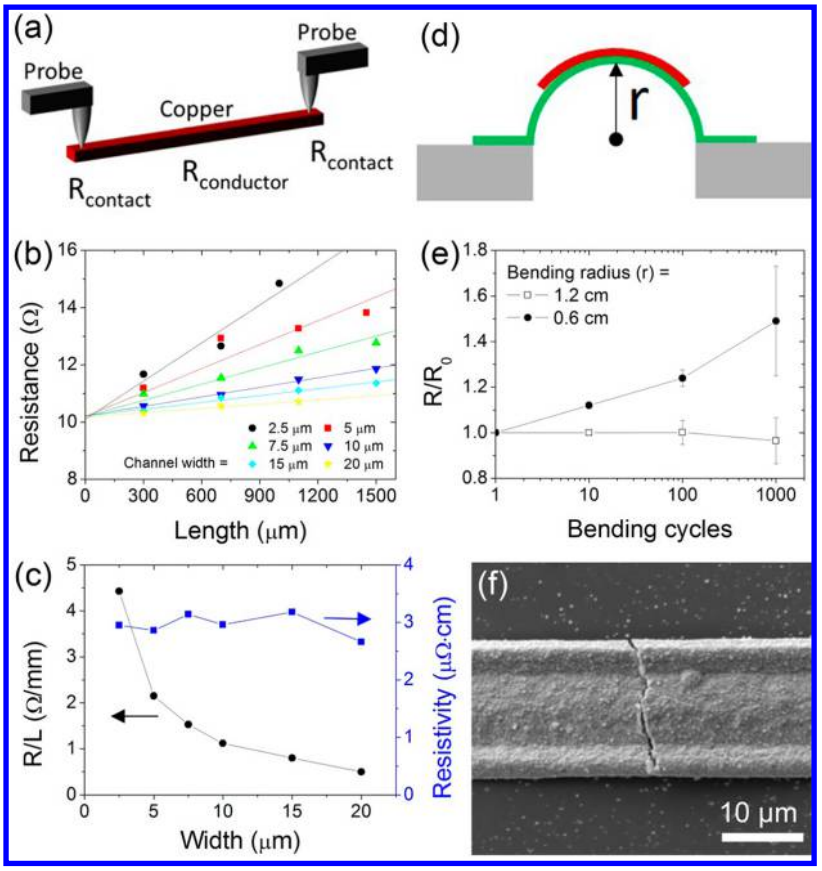

Figure 4. Electrical properties and bendability of Cu/Ag wires. (a) Schematic of the two-point probe method to measure electrical resistance of the wires. (b) Variation of wire resistance with length for different channel widths, but constant depth (4 μm). Both 2.5 and 20 μm have only three data points, because of termination of capillary flow of the Ag ink before 1.5 mm. (c) Variation of linear resistance and resistivity (derived from (b)) with channel width. The resistivity values do not show a major change over the entire range of widths. (d) Schematic depicting the experimental set up for the bending test. The substrate, attached to a stationary block and a sliding stage, is bent to a certain radius and restored to its initial state to complete one bending cycle. (e) Electrical resistance of the wires as a function of bending cycles under different bending radii (0.6 and 1.2 cm). (f) SEM showing a microcrack along the width of a wire after 1000 bending cycles at r = 0.6 cm.

0.6 and 0.1 for the 2.5 and 10 μm channels, respectively. Note that the aspect ratios can be further improved by inhibiting the side-overgrowth through the addition of special additives to the electroless plating solution.[33] The surface morphology of the plated Cu is characterized using atomic force microscopy, which revealed that the root-mean-square roughness over a 25 μm^2 area was 81.8 ± 5.2 nm (Supporting Information, Figure S4).

To study the effect of the channel geometry on the electrical properties, we used the two-point probe method (Figure 4a) to measure the resistance of the Cu/Ag wires in channels with different widths (2.5 to 20 μm) at a constant depth (4 μm). Figure 4b illustrates the resistance of all wires, irrespective of the channel width, varied linearly with length in accordance with Ohm's law, suggesting dimensional invariance of the wires along their length. The contact resistance (between the tungsten probes and the wires) was nearly independent of the wire width, which is also a signature of a true conductor. The calculated resistivity is similar for all wires, with an average value of 2.96 ± 0.1 $\mu\Omega$ cm, which translates to a conductivity of 57% of bulk Cu (Figure 4c). This is impressive considering the maximum temperature employed during the entire process was 100 °C during annealing the Ag ink. The resistance per unit length of the wire scales inversely with the channel width. For example, linear resistance almost doubles upon decreasing the channel width by a factor of 2. Despite the low line width, very low values of linear resistance (down to 1 Ω mm^{-1} for 10 μm wide channels) are achieved due to the low resistivity and high aspect ratio of the patterned wires. We also studied the effect of channel shape on resistance of the wires (Supporting Information, Figure S5). Interestingly, the resistance of wires in nonlinear channels is slightly higher than those in linear channels of the same length, which may result from thinner Ag deposits around bends in the channel.

To investigate mechanical flexibility and durability of the Cu/Ag wires, we examined the change in electrical resistance of five wires (width: 15 μm, depth: 4 μm) subjected to repeated bending cycles at two different radii of curvature (r) (Figure 4d). As shown in Figure 4e, for r of 1.2 cm (~0.4% tensile strain), electrodes subjected to 1000 repeated bending cycles exhibited only a slight increase in their electrical resistance relative to the initial value. For r of 0.6 cm (0.8% strain), the electrical resistance increased gradually, with a 1.5-fold increase after 1000 cycles. None of the patterned wires exhibited complete failure. The SEM image reveals formation of microcracks along the width of the wires, parallel to the axis of bending (Figure 4f). Although the bending performance is acceptable for most flexible electronics applications, it may be further optimized by employing thinner wires or an encapsulating layer to shift the stress-neutralization plane during bending into the Cu layer.[34] We also investigated the adhesion of the Cu/Ag wires (widths: 2.5–100 μm, depth: 4

DOI: 10.1021/am507539a
ACS Appl. Mater. Interfaces 2015, 7, 1841–1847

μm) using the scotch tape and ultrasonication tests. Although wider wires (>30 μm) showed delamination in some locations, the narrower wires displayed exceptional adhesion to the molded epoxy substrate and remained anchored to the channels even after three consecutive tests.

Figure 5 highlights the versatility of this method to produce high-resolution conductors. Figure 5a shows a top-view SEM of

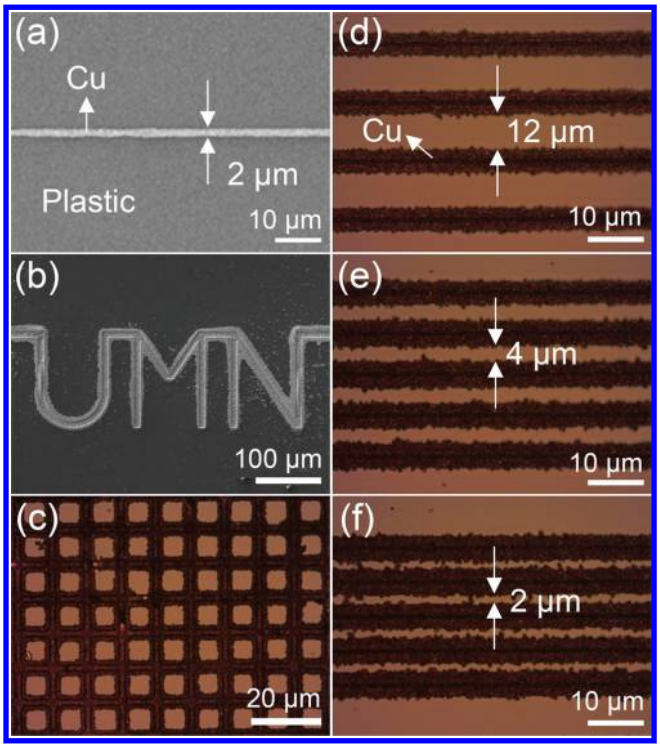

Figure 5. IPP patterning of high-resolution, complex features. SEM images of a patterned (a) 2 μm wide Cu/Ag wire and (b) UMN feature on a plastic substrate. The lighter region is metal. Optical micrographs showing (c) a crossbar pattern (line width and spacing: 5 μm) and an array of 4 μm wide lines with a spacing of (d) 12 μm, (e) 4 μm, and (f) 2 μm. Darker regions are metal. Occasional shorting in 2 μm wires is evident.

a 2 μm wide Cu/Ag line. Despite such high resolution, line consistency and sharp edge definition over a length scale of tens of microns are clearly evident. Because capillary flow is impartial to the shape of the channel, complex patterns such as "UMN" (line width: 12 μm) and crossbars (line width and spacing: 5 μm) can also be easily produced, without breaks or defects. For device applications, miniaturized line spacing is critical to performance along with line width. To determine the minimum line spacing obtainable using this approach, we fabricated an array of channels (line width and depth: 4 μm) with an initial spacing of 15, 7.5, and 5 μm. After the printing and plating steps (plating time: 15 min), the width of the individual Cu/Ag wires was 7 μm, and the spacing reduced to 12, 4, and 2 μm, respectively (Figure 5 d–f). No shorts were observed for lines with 4 μm spacing, but the 2 μm lines exhibited occasional shorting (Figure 5f). To our knowledge, such high-resolution, high-aspect ratio metal patterning of conductive features embedded in plastic substrates using an additive, liquid-based process has not been reported previously.

3. CONCLUSIONS

We have demonstrated a new approach, referred to as IPP, for patterning highly conductive wires through capillarity-induced flow of inkjet-printed reactive Ag ink into microimprinted channels on a plastic substrate followed by a Cu electroless plating step. Specifically, high-resolution metal wires with minimum line width and spacing as low as 2 and 4 μm, respectively, have been achieved using this approach. High-aspect ratio features, as high as 0.6, are obtained after the Cu deposition. The Cu/Ag wires display excellent conductivity (>50% of bulk metal), which is invariant over different channel dimensions, making them suitable candidates for flexible electronic devices and circuits. Because of their high aspect ratio and electrical conductivity, wires as fine as 2.5 μm exhibit a very low linear resistance (<5 Ω mm^{-1}). The embedded wires exhibit good flexibility and resilience, with minimal degradation in electrical performance after thousands of bending cycles. Since our patterning approach is compatible with roll-to-roll processing, it can be readily implemented in a continuous, additive manufacturing process.

4. MATERIALS AND METHODS

Master Template Fabrication. Silicon wafer (100) was first cleaned by a Piranha solution (5:1 H_2SO_4 with H_2O_2) for 20 min at 120 °C and then rinsed with deionized (DI) water and dried. The wafer was prebaked at 115 °C for 1 min. Photoresist (Shipley 1813) was spin-coated (3000 rpm) on the silicon wafer for 30 s, followed by softbake at 110 °C for 1 min to drive off solvents. A predesigned mask was placed above the photoresist-coated silicon wafer and exposed to UV light for 5 s in an ultraviolet exposing system (Karl Suss MABA6). The silicon wafer was immersed in the developer solution for 1 min, rinsed with DI water, and dried. The patterned silicon wafer was then dry-etched to a required depth by reactive ion etching (SLR 770 Deep Trench Etcher). The etch rate was 0.9 μm min^{-1}. Lastly, the patterned silicon wafer with reservoirs and channels was washed in acetone and isopropyl alcohol to remove the photoresist and rinsed with DI water. The patterned silicon wafer was placed in a hexamethyldisilazane (HMDS) vapor bath for 2 h.

Polydimethylsiloxane Stamp Fabrication. For preparing the PDMS stamp, PDMS monomer and its curing agent (Dow Corning, Sylgard-184) were thoroughly mixed in a 10:1 weight ratio, respectively, and vacuum-degassed for 30 min. The master template substrate was placed in a plastic Petri dish, and 30 g of the PDMS prepolymer mixture was poured over the substrate and allowed to level out. The prepolymer mixture was then cured in an atmospheric oven at 60 °C for 12 h. After completely curing, the PDMS stamp was delaminated from the silicon master template. The stamp was then placed in an oven at 120 °C for 2 h to enhance its modulus.

Imprinted Flexible Substrate Fabrication. A 25 μm thick coating of a flexible, UV-curable polymer, NOA-73 (Norland Products Inc.), was applied to a 75 μm thick PET substrate. Prior to the coating, the PET substrate was air–plasma treated for 3 min to promote the adhesion of the coating. The PDMS stamp was inserted into the liquid coating and pressed using a glass roller to drive out any entrapped air bubbles at the coating–stamp interface. The coating was cured by exposure to UV light for 20 min. Following complete cure, the stamp was delaminated, leaving behind imprinted features in the NOA/PET substrate.

Inkjet Printing of Ag Ink. An 80 μm diameter drop-on-demand inkjet nozzle was employed for printing the Ag ink. The optimized waveform consisted of a rise time of 5 μs, dwell time of 20 μs, fall time of 5 μs, drive voltage of 100 V, and jetting frequency of 360 Hz. The diameter of a single ejected droplet was ~65–75 μm. The nozzle was aligned to an imprinted reservoir, and a fixed number of droplets was delivered to the reservoir. Prior to printing, the imprinted substrate was air–plasma treated for 3 min for surface-energy enhancement to

DOI: 10.1021/am507539a
ACS Appl. Mater. Interfaces 2015, 7, 1841–1847

facilitate capillary flow. The printed substrate was annealed on a hot plate at 100 °C for 5 min.

Cu Electroless Plating. The Cu electroless plating solution contained 2.704 g of $CuSO_4 \cdot 5H_2O$, 8.15 g of ethylenediaminetetraacetic acid disodium salt, 3.25 g of NaOH, 100 mL of DI water, and 25 mL of an aqueous solution of formaldehyde (37% by weight). The temperature of the bath was maintained at 55 °C. The printed substrate was kept in the bath for a known amount of time and taken out, rinsed with DI water, and dried using an air gun.

■ ASSOCIATED CONTENT

Supporting Information

Reactive Ag ink properties; fabrication scheme of Si master template and PDMS daughter stamp; optical micrographs of a reservoir and a channel during different stages in the IPP process; schematic of the experimental setup for investigating the influence of channel geometry on Ag ink travel length; surface characterization of electroless plated Cu; and effect of channel shape on electrical resistance of the wires. This material is available free of charge via the Internet at http://pubs.acs.org.

■ AUTHOR INFORMATION

Corresponding Authors

*E-mail: frisbie@umn.edu. (C.D.F.)
*E-mail: lfrancis@umn.edu. (L.F.F.)

Author Contributions

§A.M. and W.J.H. contributed equally. The manuscript was written through contributions of all authors. All authors have given approval to the final version of the manuscript.

Notes

The authors declare no competing financial interest.

■ ACKNOWLEDGMENTS

This work was supported by the Multi-University Research Initiative (MURI) program sponsored by the Office of Naval Research (MURI Award No. N00014-11-1-0690). The authors thank Prof. S. Kumar and D. Barton for useful discussions. Parts of this work were carried out at the Characterization Facility and the Nanofabrication Center of the University of Minnesota.

■ REFERENCES

(1) Arias, A. C.; MacKenzie, J. D.; McCulloch, I.; Rivnay, J.; Salleo, A. Materials and Applications for Large Area Electronics: Solution-Based Approaches. *Chem. Rev.* **2010**, *110*, 3−24.
(2) Sokolov, A. N.; Roberts, M. E.; Bao, Z. Fabrication of Low-Cost Electronic Biosensors. *Mater. Today* **2009**, *12*, 12−20.
(3) Briand, D.; Oprea, A.; Courbat, J.; Bârsan, N. Making Environmental Sensors on Plastic Foil. *Mater. Today* **2011**, *14*, 416−423.
(4) Khodagholy, D.; Doublet, T.; Gurfinkel, M.; Quilichini, P.; Ismailova, E.; Leleux, P.; Herve, T.; Sanaur, S.; Bernard, C.; Malliaras, G. G. Highly Conformable Conducting Polymer Electrodes for in Vivo Recordings. *Adv. Mater.* **2011**, *23*, H268−H272.
(5) Galagan, Y.; J.M. Rubingh, J.-E.; Andriessen, R.; Fan, C.-C.; W.M. Blom, P.; C. Veenstra, S.; M. Kroon, J. ITO-Free Flexible Organic Solar Cells with Printed Current Collecting Grids. *Sol. Energy Mater. Sol. Cells* **2011**, *95*, 1339−1343.
(6) Facchetti, A.; Yoon, M.-H.; Marks, T. J. Gate-Planarized Low-Operating Voltage Organic Field-Effect Transistors Enabled by Hot Polymer Pressing/Embedding of Conducting Metal Lines. *J. Am. Chem. Soc.* **2006**, *128*, 4928−4929.
(7) Hines, D. R.; Ballarotto, V. W.; Williams, E. D.; Shao, Y.; Solin, S. A. Transfer Printing Methods for the Fabrication of Flexible Organic Electronics. *J. Appl. Phys.* **2007**, *101*, 024503−9.
(8) Mahajan, A.; Francis, L. F.; Frisbie, C. D. Facile Method for Fabricating Flexible Substrates with Embedded, Printed Silver Lines. *ACS Appl. Mater. Interfaces* **2013**, *6*, 1306−1312.
(9) Moonen, P. F.; Yakimets, I.; Huskens, J. Fabrication of Transistors on Flexible Substrates: From Mass-Printing to High-Resolution Alternative Lithography Strategies. *Adv. Mater.* **2012**, *24*, 5526−5541.
(10) Kang, H.; Kitsomboonloha, R.; Jang, J.; Subramanian, V. High-Performance Printed Transistors Realized Using Femtoliter Gravure-Printed Sub-10 Mm Metallic Nanoparticle Patterns and Highly Uniform Polymer Dielectric and Semiconductor Layers. *Adv. Mater.* **2012**, *24*, 3065−3069.
(11) Kitsomboonloha, R.; Morris, S. J. S.; Rong, X.; Subramanian, V. Femtoliter-Scale Patterning by High-Speed, Highly Scaled Inverse Gravure Printing. *Langmuir* **2012**, *28*, 16711−16723.
(12) Fukuda, K.; Sekine, T.; Kumaki, D.; Tokito, S. Profile Control of Inkjet Printed Silver Electrodes and Their Application to Organic Transistors. *ACS Appl. Mater. Interfaces* **2013**, *5*, 3916−20.
(13) Perelaer, J.; Smith, P. J.; Mager, D.; Soltman, D.; Volkman, S. K.; Subramanian, V.; Korvink, J. G.; Schubert, U. S. Printed Electronics: The Challenges Involved in Printing Devices, Interconnects, and Contacts Based on Inorganic Materials. *J. Mater. Chem.* **2010**, *20*, 8446−8453.
(14) van Osch, T. H. J.; Perelaer, J.; de Laat, A. W. M.; Schubert, U. S. Inkjet Printing of Narrow Conductive Tracks on Untreated Polymeric Substrates. *Adv. Mater.* **2008**, *20*, 343−345.
(15) Walker, S. B.; Lewis, J. A. Reactive Silver Inks for Patterning High-Conductivity Features at Mild Temperatures. *J. Am. Chem. Soc.* **2012**, *134*, 1419−1421.
(16) Mahajan, A.; Frisbie, C. D.; Francis, L. F. Optimization of Aerosol Jet Printing for High-Resolution, High-Aspect Ratio Silver Lines. *ACS Appl. Mater. Interfaces* **2013**, *5*, 4856−4864.
(17) Sekitani, T.; Noguchi, Y.; Zschieschang, U.; Klauk, H.; Someya, T. Organic Transistors Manufactured Using Inkjet Technology with Subfemtoliter Accuracy. *Proc. Natl. Acad. Sci. U.S.A.* **2008**, *105*, 4976−4980.
(18) Guo, L. J. Nanoimprint Lithography: Methods and Material Requirements. *Adv. Mater.* **2007**, *19*, 495−513.
(19) Singh, M.; Haverinen, H. M.; Dhagat, P.; Jabbour, G. E. Inkjet Printing—Process and Its Applications. *Adv. Mater.* **2010**, *22*, 673−685.
(20) Mallory, G. O.; Hajdu, J. B. *Electroless Plating: Fundamentals and Applications;* American Electroplaters and Surface Finishers Society: Orlando, FL, 1990.
(21) Hendriks, C. E.; Smith, P. J.; Perelaer, J.; van den Berg, A. M. J.; Schubert, U. S. Invisible" Silver Tracks Produced by Combining Hot-Embossing and Inkjet Printing. *Adv. Funct. Mater.* **2008**, *18*, 1031−1038.
(22) Yu, J. S.; Kim, I.; Kim, J. S.; Jo, J.; Larsen-Olsen, T. T.; Sondergaard, R. R.; Hosel, M.; Angmo, D.; Jorgensen, M.; Krebs, F. C. Silver Front Electrode Grids for ITO-Free All Printed Polymer Solar Cells with Embedded and Raised Topographies, Prepared by Thermal Imprint, Flexographic and Inkjet Roll-to-Roll Processes. *Nanoscale* **2012**, *4*, 6032−40.
(23) Yu, J.-S.; Jung, G. H.; Jo, J.; Kim, J. S.; Kim, J. W.; Kwak, S.-W.; Lee, J.-L.; Kim, I.; Kim, D. Transparent Conductive Film with Printable Embedded Patterns for Organic Solar Cells. *Sol. Energy Mater. Sol. Cells* **2013**, *109*, 142−147.
(24) Dong, M.; Chatzis, I. The Imbibition and Flow of a Wetting Liquid Along the Corners of a Square Capillary Tube. *J. Colloid Interface Sci.* **1995**, *172*, 278−288.
(25) Juncker, D.; Schmid, H.; Drechsler, U.; Wolf, H.; Wolf, M.; Michel, B.; de Rooij, N.; Delamarche, E. Autonomous Microfluidic Capillary System. *Anal. Chem.* **2002**, *74*, 6139−6144.
(26) Hartnett, J. P.; Kostic, M. Heat Trsanfer to Newtonian and Non-Newtonian Fluids In Rectangular Ducts. *Adv. Heat Transfer* **1989**, *19*, 247−356.
(27) Washburn, E. W. The Dynamics of Capillary Flow. *Phys. Rev.* **1921**, *17* (3), 273.

DOI: 10.1021/am507539a
ACS Appl. Mater. Interfaces 2015, 7, 1841−1847

(28) Hansen, C. J.; Saksena, R.; Kolesky, D. B.; Vericella, J. J.; Kranz, S. J.; Muldowney, G. P.; Christensen, K. T.; Lewis, J. A. High-Throughput Printing Via Microvascular Multinozzle Arrays. *Adv. Mater.* **2013**, *25*, 96−102.
(29) Yang, D.; Krasowska, M.; Priest, C.; Popescu, M. N.; Ralston, J. Dynamics of Capillary-Driven Flow in Open Microchannels. *J. Phys. Chem. C* **2011**, *115*, 18761−18769.
(30) Deegan, R. D.; Bakajin, O.; Dupont, T. F.; Huber, G.; Nagel, S. R.; Witten, T. A. Capillary Flow as the Cause of Ring Stains from Dried Liquid Drops. *Nature* **1997**, *389*, 827−829.
(31) Price, K. K.; McCormick, A. V.; Francis, L. F. CryoSEM Investigation of Latex Coatings Dried in Walled Substrates. *Langmuir* **2012**, *28*, 10329−10333.
(32) Jung, Y.; Kajiya, T.; Yamaue, T.; Doi, M. Film Formation Kinetics in the Drying Process of Polymer Solution Enclosed by Bank. *Jpn. J. Appl. Phys.* **2009**, *48*, 031502.
(33) Hasegawa, M.; Okinaka, Y.; Shacham-Diamand, Y.; Osaka, T. Void-Free Trench-Filling by Electroless Copper Deposition Using the Combination of Accelerating and Inhibiting Additives. *Electrochem. Solid-State Lett.* **2006**, *9*, C138−C140.
(34) Guo, R.; Yu, Y.; Xie, Z.; Liu, X.; Zhou, X.; Gao, Y.; Liu, Z.; Zhou, F.; Yang, Y.; Zheng, Z. Matrix-Assisted Catalytic Printing for the Fabrication of Multiscale, Flexible, Foldable, and Stretchable Metal Conductors. *Adv. Mater.* **2013**, *25*, 3343−3350.

DOI: 10.1021/am507539a
ACS Appl. Mater. Interfaces 2015, 7, 1841−1847